ACS APPLIED MATERIALS & INTERFACES

Letter

www.acsami.org

Graphene-Supported Nickel–Platinum Nanoparticles as Efficient Catalyst for Hydrogen Generation from Hydrous Hydrazine at Room Temperature

Yeshuang Du,[†] Jun Su,[§] Wei Luo,*[,†,‡] and Gongzhen Cheng*[,†]

[†]College of Chemistry and Molecular Sciences, Wuhan University, Wuhan, Hubei 430072, P. R. China

[‡]Suzhou Institute of Wuhan University, Suzhou, Jiangsu 215123, P. R. China

[§]Wuhan National Laboratory for Optoelectronics, Huazhong University of Science and Technology, Wuhan, Hubei 430074, P. R. China

Supporting Information

ABSTRACT: Ultrafine monodisperse bimetallic NiPt nanoparticles with different compositions have been successfully synthesized by coreduction of nickel acetylacetonate and platinum acetylacetonate with borane-*tert*-butylamine in oleylamine. Among all the catalysts tested, $Ni_{84}Pt_{16}$/graphene exhibited 100% hydrogen selectivity, and marked high catalytic activity, with TOF values of 415 h^{-1} at 50 °C, and 133 h^{-1} at 25 °C for hydrogen generation from alkaline solution of hydrazine.

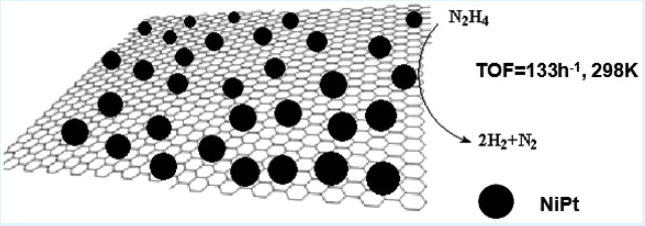

KEYWORDS: *monodisperse, Ni, Pt, hydrazine, hydrogen storage*

Hydrogen, producing only water as a byproduct, has emerged as one of the potential carbon-neutral energy carrier alternatives. Storage of hydrogen as a compressed gas is the current state-of-the-art, but to avoid the risk of high pressures and increase the storage density, numerous hydrogen storage approaches are currently under investigation.[1−3] The liquid-phase hydrogen storage materials, which are easy to handle and transport by taking advantage of the existing liquid-based distribution channels, without the involvement of any solid byproduct, have been considered more advantageous over traditional solid-phase hydrogen storage materials. There are several potential liquid-phase hydrogen storage materials that have received recent attention, including formic acid (HCOOH),[4] liquid organic hydrogen carriers (LOHCs),[5] liquid amine borane complexes,[6] and hydrous hydrazine ($N_2H_4{\cdot}H_2O$).[7−11] Among them, hydrous hydrazine has been identified as a potential hydrogen carrier for portable hydrogen storage application due to its high hydrogen content (8.0 wt %), convenient transportation and production of only nitrogen as byproduct, which does not need on-board collection for recycling, in addition to hydrogen via a complete decomposition way (eq 1). Moreover, nitrogen could be transformed to ammonia and then to hydrazine successively by electrolytic process to fulfill the easy recharging.[8] However, from a perspective of hydrogen storage, the undesirable dehydrogenation way (eq 2) should be avoided, as NH_3 is toxic to the fuel cell catalysts.[9] To this end, a number of noble and non-noble metal containing nanocatalysts have been developed recently (Table S1 in the Supporting Information); however, catalysts possessing prominent activity and selectivity at room temperature are still few, which limits their practical application.

$$N_2H_4 \rightarrow N_2 + 2H_2 \quad (1)$$

$$3N_2H_4 \rightarrow 4NH_3 + N_2 \quad (2)$$

Recently, binary NiPt alloy nanoparticles (NPs) have been found to be efficient catalysts toward dehydrogenation of hydrous hydrazine in alkaline solution. For example, Xu's group reported the NiPt nanocatalysts by coreduction of nickel and platinum chlorides in the presence of CTAB with an initial turnover frequency (TOF) of 7.9 h^{-1} at room temperature,[10] and bimetallic Ni−Pt dendrimer-encapsulated NPs with TOF of 240 h^{-1} at 70 °C.[11] Yan and co-workers reported an in situ synthesis of amorphous NiPt NPs supported on Ce_2O_3 with TOF of 28.1 h^{-1} at room temperature,[12] Zhang and co-workers reported surface modification of Ni/Al_2O_3 with Pt exhibit a TOF value of 16.5 h^{-1} at 30 °C.[13] Our group reported in situ synthesis of graphene supported flower-like NiPt nanoclusters with TOF of 68 h^{-1} at room temperature.[14] It has been reported that the ultrafine metal NPs with a narrow size distribution and high dispersion may be conductive to their catalytic performance.[15] Consideration the limitation seen from previous reports in controlling size and distribution, the control synthesis of well dispersed metal NPs coupling with these merits, and further discovering their intrinsically catalytic

Received: October 5, 2014
Accepted: January 6, 2015
Published: January 6, 2015

DOI: 10.1021/am5068436
ACS Appl. Mater. Interfaces 2015, 7, 1031−1034

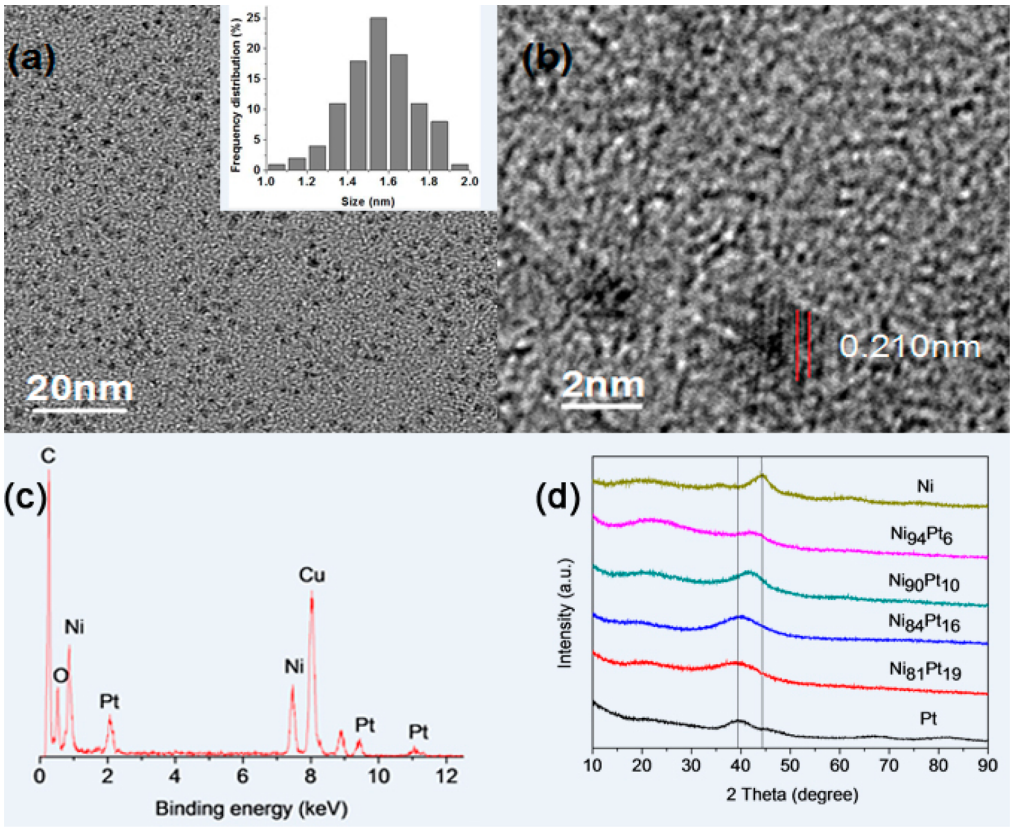

Figure 1. (a, b) TEM images and (c) EDX spectra of $Ni_{84}Pt_{16}$ and (d) XRD patterns of NiPt with different composition, pure Ni, and Pt.

activity toward hydrogen generation from hydrazine at relatively low temperature are highly desirable. Our very recent report showed a facile liquid impregnation method for immobilization of ultrafine NiPt NPs inside the pores of metal−organic frameworks (MIL-101). The size and distribution of NiPt NPs could be controlled by the pores of MIL-101, which result in exceedingly high catalytic activity toward dehydrogenation of hydrous hydrazine with TOF of 62.5 h^{-1} at room temperature.[16] Recently, amine boranes have been normally used as reducing agents in oleylamine for controlled synthesis of monodisperse metal nanocrystallites with high catalytic activities.[17] In the light of these results, herein, we report a facile synthesis of monodisperse NiPt NPs with low noble-metal containing, and their catalytic activity toward hydrogen generation from alkaline solution of hydrazine under ambient conditions at 50 and 25 °C, respectively. Graphene, a single layer of sp^2 carbon lattices, with many advantages such as large specific surface area, high intrinsic mobility, large free electrons density, etc.,[18] was chosen as catalyst support for anchoring NiPt NPs with good dispersion. As expected, the resultant $Ni_{84}Pt_{16}$/graphene exhibits 100% hydrogen selectivity and exceedingly high catalytic activity with turnover frequency (TOF) values of 415 h^{-1} at 50 °C and 133 h^{-1} at 25 °C for hydrogen generation from alkaline solution of hydrazine under ambient conditions, respectively.

The monodisperse NiPt alloy NPs were synthesized by coreduction of nickel acetylacetonate ($Ni(acac)_2$) and platinum acetylacetonate ($Pt(acac)_2$) with borane-*tert*-butylamine complex (BTB) in oleylamine (OAm) at 90 °C. In the reaction, OAm served both as the solvent and surfactant, and BTB acted as a reducing agent. The compositions of the NiPt NPs were controlled by varying the initial molar ratio of $Ni(acac)_2$ and $Pt(acac)_2$, and further analyzed by inductively coupled plasma-atomic emission spectroscopy (ICP-AES) (see Table S2 in the Supporting Inforation). The microstructures of the as-synthesized NiPt NPs with different compositions were characterized by transmission electron microscopy (TEM) as shown in Figure 1 and Figure S1 in the Supporting Information. The NiPt NPs have a narrow size distribution with a mean particle size of 1.6 ± 0.2 nm. A representative high-resolution TEM (HRTEM) image of $Ni_{84}Pt_{16}$ in Figure 1b revealed the *d*-spacing of 0.210 nm, which is larger than the (111) spacing of face-centered cubic (fcc) Ni (0.204 nm) and smaller than that of Pt (0.227 nm), suggesting that NiPt is formed as an alloy structure. The energy dispersive X-ray (EDX) spectra in Figure 1c further confirm the coexistence of Ni and Pt. Figure 1d is the powder X-ray diffraction (PXRD) patterns of the as-synthesized Ni, Pt and NiPt NPs. It is clear that with the Pt amount increased, the (111) peak shifts to a lower angle toward Pt (111) because of the increase of the lattice parameters, indicating that NiPt is formed as an alloy. The X-ray photoelectron spectroscopy (XPS) spectra in Figure S2 in the Supporting Information show the characteristic signals for Ni and Pt, indicating the coexistence of both metals. The formation of oxidized Ni most likely occurs during the sample preparation process for the XPS experiment. As a result, the $2p_{2/3}$ peak of Ni appearing at 856.2 eV is higher than that of metallic Ni^0 (852.7 eV).[14] The effect of Pt toward Ni is negligible compared to oxygen influence. It showed that the signals of Pt in NiPt alloy were a little different from that of pure Pt. The 4f peaks of Pt in $Ni_{84}Pt_{16}$/graphene shifted 0.78 eV to higher binding energies in contrast to that of Pt/graphene, indicating Ni has electron interaction toward Pt. It can be inferred that the electron structure of catalyst surface is

DOI: 10.1021/am5068436
ACS Appl. Mater. Interfaces 2015, 7, 1031−1034

changed by alloying Ni with Pt. The change may affect the bonding form of catalyst surface to N_2H_4 or other reaction intermediates, and thus the catalytic activity and H_2 selectivity of NiPt are improved.[9]

To study their catalytic performance, we deposited the as-synthesized NiPt NPs on graphene by sonicating the mixture of graphene and NiPt NPs in hexane dispersion for 2 h, followed by washed with ethanol and dried under vacuum. To activate these NiPt NPs, we tested the acetic acid treatment and thermal treatment; however, they are both inferior to that of simple ethanol wash, which should be explained by further work. As shown in the TEM image in Figure S3 in the Supporting Information, the NiPt NPs are well-dispersed on graphene and maintained their particle size distribution. The catalytic performance of NiPt/graphene with different compositions, together with Ni/graphene and Pt/graphene for hydrogen generation from aqueous solution of hydrazine at 50 °C in the presence of NaOH (0.5 M) are shown in Figure 2. Neither Ni

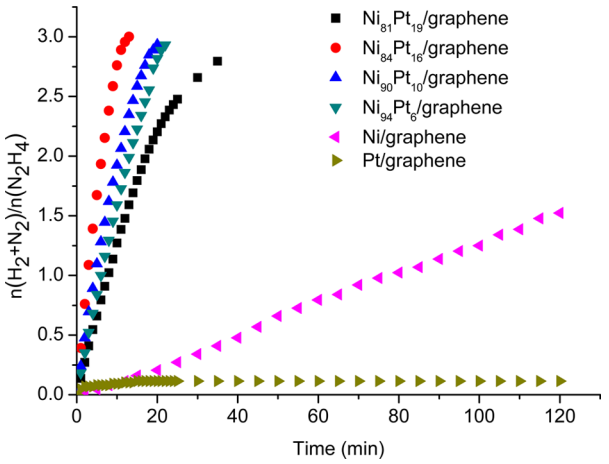

Figure 2. Time course plots for the decomposition of hydrazine over NiPt/graphene, Ni/graphene, Pt/graphene in NaOH solution (0.5 M) at 50 °C (catalyst = 50 mg; $N_2H_4{\cdot}H_2O$ = 0.1 mL).

nor Pt is catalytic active, however, by alloying small amount of Pt to Ni, the catalytic activity and selectivity of the catalysts increased obviously, indicating the molecular-scale synergy of Ni−Pt alloy. Among all the bimetallic NiPt/graphene catalysts investigated, $Ni_{84}Pt_{16}$/graphene exhibits the highest catalytic activity with the TOF value of 415 h^{-1}, which is the higher than most of the reported values (see Table S1 in the Supporting Information). To our delight, even at 25 °C, the $Ni_{84}Pt_{16}$/graphene exhibits 100% hydrogen selectivity with a TOF value as high as 133 h^{-1}. The drastic catalytic activity enhancement of these monodisperse 1.6 nm NiPt NPs is likely caused by their ultrafine size, narrow size distribution and the synergistic effect between Ni and Pt in the alloy structure, which is consistent with what was observed on other binary alloy systems.[10−17] This result can be explained by the Sabatier principle, which claim that the catalytic activity can be controlled by the catalytic surface.[18] Therefore, there is an optimal ratio between Ni and Pt to show neither too weak nor too strong binding to the hydrazine, which may result in the highest catalytic activity. The hydrogen selectivity is further confirmed by mass spectroscopy, as shown in Figure S4 in the Supporting Information, only the mixture of H_2 and N_2 but no NH_3 has been detected, indicating the excellent hydrogen selectivity for hydrogen generation from hydrazine by the as-synthesized NiPt/graphene catalysts. For comparison, NiPt NPs without support have been synthesized, and their catalytic activity toward dehydrogenation of hydrazine was tested. As shown in Figure S5 in the Supporting Information, their catalytic activity and hydrogen selectivity are both inferior to those of NiPt NPs supported on graphene, whereas graphene exhibit no catalytic activity, highlighting the positive effect of utilization graphene as a two-dimensional support in facilitating the electron transfer and mass transport.[19] It is known that NaOH has a great effect on the catalytic activity of nanocatalysts. We tested the hydrogen generation from hydrazine solution with/without adding NaOH. As shown in Figure S6 in the Supporting Information, the gas released from hydrazine can reach a stoichiometric amount (3 equiv) in 13 min with NaOH (0.5 M) at 323 K, whereas the dehydrogenation is incomplete and slow without NaOH, which is consistent with the reported results.[10−14] The reason is that NaOH can accelerate the rate-determining step ($N_2H_4 \rightarrow N_2H_3{*}+H{*}$) of hydrazine decomposition[19] and alkaline NaOH suppresses the formation of basic NH_3.[20] Furthermore, in order to further tune and improve the catalytic activity performance, we prepared a series of graphene-supported MPt (M = Cu, Fe, Co) and NiX (X = Au, Ag, Pd) NPs, and investigated their catalytic activity for dehydrogenation hydrazine (see Figures S7 and S8 in the Supporting Information). Compared with other bimetallic catalysts ($Ni_{13}Au_{87}$, $Ni_{89}Ag_{11}$, $Ni_{68}Pd_{32}$, $Cu_{82}Pt_{18}$, $Fe_{60}Pt_{40}$, and $Co_{75}Pt_{25}$), the kinetics rate of hydrous hydrazine catalyzed by $Ni_{84}Pt_{16}$/graphene is faster than most catalysts except for $Co_{75}Pt_{25}$/graphene. However, only 2.1 equiv of gas can be released from hydrous hydrazine catalyzed by $Co_{75}Pt_{25}$/graphene with 66% hydrogen selectivity, which is similar to Yan's result about CeO_x-supported CoPt.[21]

To obtain the activity energy (E_a) of the dehydrogenation of hydrazine catalyzed by $Ni_{84}Pt_{16}$/graphene, we carried out the catalytic reactions at different temperatures in the range of 25 to 60 °C (Figure 3). The values of rate constant k at different temperatures were calculated from the slope of the linear part of each plot from Figure 3. The inset in Figure 3 is Arrhenius plot of ln k vs $1/T$, from which the apparent activity energy was

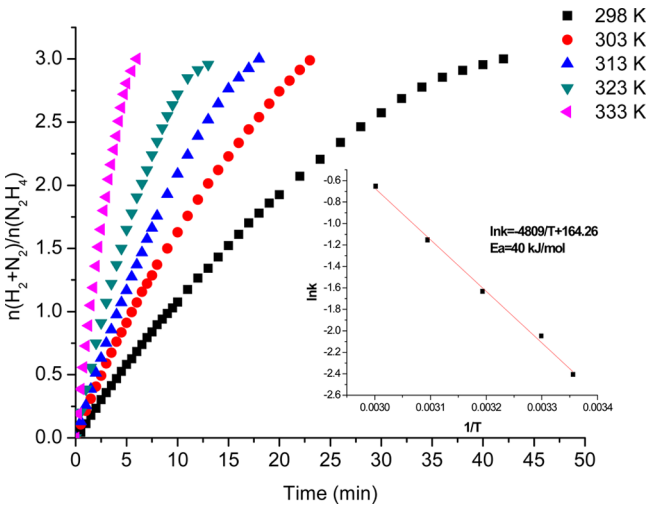

Figure 3. Time course plots for hydrogen generation by the decomposition of hydrazine catalyzed by 50 mg of $Ni_{84}Pt_{16}$/graphene at 25, 30, 40, 50, and 60 °C, and (inset) Arrhenius plot of lnk vs $1/T$.

DOI: 10.1021/am5068436
ACS Appl. Mater. Interfaces 2015, 7, 1031−1034

determined to be 40 kJ/mol. This value was smaller than most reported data (see Table S1 in the Supporting Information).

The reusability of $Ni_{84}Pt_{16}$/graphene catalyst was also tested by successively adding the same amount of hydrous hydrazine after the completion of the previous run at 25 and 50 °, respectively. As shown in Figure S9 in the Supporting Information, there was a slight decrease in catalytic activity after 3 cycles, but the hydrogen selectivity was not changed. The XRD patterns of $Ni_{84}Pt_{16}$/graphene before and after cycling test at 25 °C showed no distinct difference, as shown in Figure S10 in the Supporting Information. But the TEM image demonstrated some nanoparticles are ready to aggregate after the cycling, which could explain the slight decrease of catalytic activity. Further work on the enhancement of the stability of the as-synthesized catalyst for hydrogen generation from hydrazine is underway.

In summary, ultrafine monodisperse NiPt alloy NPs have been successfully synthesized by coreduction of nickel acetylacetonate and platinum acetylacetonate with BTB in oleylamine at 90 °C. The compositions of NiPt NPs were controlled by varying the initial molar ratios of metal precursors. The NiPt NPs were deposited on graphene and tested for their catalytic dehydrogenation of alkaline solution of hydrazine under ambient condition. Among all the catalysts tested, $Ni_{84}Pt_{16}$/graphene exhibits 100% hydrogen selectivity, and marked high catalytic activity, with TOF values of 415 h^{-1} at 50 °C and 133 h^{-1} at 25 °C, which are higher than most of the reported values. The metal component control synthesis of ultrafine alloy NPs with narrow size distribution is believed to strongly promote the practical application of hydrous hydrazine as a hydrogen storage material.

■ ASSOCIATED CONTENT

Supporting Information

Detailed experiment process and Figures S1−S10 and Table S1−S2 as mentioned in the text. This material is available free of charge via the Internet at http://pubs.acs.org.

■ AUTHOR INFORMATION

Corresponding Authors

*E-mail: wluo@whu.edu.cn. Tel.: +86 2768752366.
*E-mail: gzcheng@whu.edu.cn.

Notes

The authors declare no competing financial interest.

■ ACKNOWLEDGMENTS

This work was financially supported by the National Natural Science Foundation of China (21201134), the Natural Science Foundation of Jiangsu Province(BK20130370), the Natural Science Foundation of Hubei Province(2013CFB288), the Creative Research Groups of Hubei Province (2014CFA007), and Large-scale Instrument and Equipment Sharing Foundation of Wuhan University.

■ REFERENCES

(1) Graetz, J. New Approaches to Hydrogen Storage. *Chem. Soc. Rev.* **2009**, *38*, 73−82.
(2) Li, S. L.; Xu, Q. Metal-Organic Frameworks as Platforms for Clean Energy. *Energy Environ. Sci.* **2013**, *6*, 1656−1683.
(3) Staubitz, A.; Robertson, A. P. M.; Manners, I. Ammonia-Borane and Related Compounds as Dihydrogen Sources. *Chem. Rev.* **2010**, *110*, 4079−4124.
(4) Grasemann, M.; Laurenczy, G. Formic Acid as a Hydrogen Source-Recent Developments and Future Trends. *Energy Environ. Sci.* **2012**, *5*, 8171−8181.
(5) Teichmann, D.; Stark, K.; Mueller, K.; Zöttl, G.; Wasserscheid, P.; Arlt, W. Energy Storage in Residential and Commercial Buildings via Liquid Organic Hydrogen Carriers (LOHC). *Energy Environ. Sci.* **2012**, *5*, 9044−9054.
(6) Luo, W.; Campbell, P. G.; Zakharov, L. N.; Liu, S. Y. A Single-Component Liquid-Phase Hydrogen Storage Material. *J. Am. Chem. Soc.* **2011**, *133*, 19326−19329.
(7) Tong, D. G.; Chu, W.; Wu, P.; Gu, G. F.; Zhang, L. Mesoporous Multiwalled Carbon Nanotubes as Supports for Monodispersed Iron-Boron Catalysts: Improved Hydrogen Generation from Hydrous Hydrazine Decomposition. *J. Mater. Chem. A* **2013**, *1*, 358−366.
(8) Yadav, M.; Xu, Q. Liquid-Phase Chemical Hydrogen Storage Materials. *Energy Environ. Sci.* **2012**, *5*, 9698−9725.
(9) Singh, S. K.; Xu, Q. Nanocatalysts for Hydrogen Generation from Hydrazine. *Catal. Sci. Technol.* **2013**, *3*, 1889−1900.
(10) Singh, S. K.; Xu, Q. Bimetallic Ni-Pt Nanocatalysts for Selective Decomposition of Hydrazine in Aqueous Solution to Hydrogen at Room Temperature for Chemical Hydrogen Storage. *Inorg. Chem.* **2010**, *49*, 6148−6152.
(11) Aranishi, K.; Singh, A. K.; Xu, Q. Dendrimer-Encapsulated Bimetallic Pt-Ni Nanoparticles as Highly Efficient Catalysts for Hydrogen Generation from Chemical Hydrogen Storage Materials. *ChemCatChem.* **2013**, *5*, 2248−2252.
(12) Wang, H. L.; Yan, J. M.; Wang, Z. L.; Song, O.; Jiang, Q. Highly Efficient Hydrogen Generation from Hydrous Hydrazine over Amorphous $Ni_{0.9}Pt_{0.1}/Ce_2O_3$ Nanocatalyst at Room Temperature. *J. Mater. Chem. A* **2013**, *1*, 14957−14962.
(13) He, L.; Huang, Y. Q.; Wang, A. Q.; Liu, Y.; Liu, X. Y.; Chen, X. W.; Delgado, J. J.; Wang, X. D.; Zhang, T. Surface Modification of Ni/Al_2O_3 with Pt: Highly Efficient Catalysts for H_2 Generation via Selective Decomposition of Hydrous Hydrazine. *J. Catal.* **2013**, *298*, 1−9.
(14) Cao, N.; Yang, L.; Du, C.; Su, J.; Luo, W.; Cheng, G. Z. Highly Efficient Dehydrogenation of Hydrazine over Graphene Supported Flower-like Ni-Pt Nanoclusters at Room Temperature. *J. Mater. Chem. A* **2014**, *2*, 14344−14347.
(15) Guo, S. J.; Sun, S. H. FePt Nanoparticles Assembled on Graphene as Enhanced Catalyst for Oxygen Reduction Reaction. *J. Am. Chem. Soc.* **2012**, *134*, 2492−2495.
(16) Cao, N.; Yang, L.; Dai, H. M.; Liu, T.; Su, J.; Wu, X. J.; Luo, W.; Cheng, G. Z. Immobilization of Ultrafine Bimetallic Ni-Pt Nanoparticles Inside the Pores of Metal-Organic Frameworks as Efficient Catalysts for Dehydrogenation of Alkaline Solution of Hydrazine. *Inorg. Chem.* **2014**, *53*, 10122−10128.
(17) Du, C.; Liao, Y. X.; Hua, X.; Luo, W.; Chen, S. L.; Cheng, G. Z. Amine−borane Assisted Synthesis of Wavy Palladium Nanorods on Graphene as Efficient Catalysts for Formic Acid Oxidation. *Chem. Commun.* **2014**, *50*, 12843−12846.
(18) Demirci, U. B.; Garin, F. Ru-Based Bimetallic Alloys for Hydrogen Generation by Hydrolysis of Sodium Tetrahydroborate. *J. Alloys Compd.* **2008**, *463*, 107−111.
(19) Wang, J.; Zhang, X. B.; Wang, Z.-L.; Wang, L. M.; Zhang, Y. Rhodium-Nickel Nanoparticles Grown on Graphene as Highly Efficient Catalyst for Complete Decomposition of Hydrous Hydrazine at Room Temperature for Chemical Hydrogen Storage. *Energy Environ. Sci.* **2012**, *5*, 6885−6888.
(20) Singh, S. K.; Singh, A. K.; Aranishi, K.; Xu, Q. Noble-Metal-Free Bimetallic Nanoparticle-Catalyzed Selective Hydrogen Generation from Hydrous Hydrazine for Chemical Hydrogen Storage. *J. Am. Chem. Soc.* **2011**, *133*, 19638−19641.
(21) Song, O.; Yan, J. M.; Wang, H. L.; Wang, Z. L.; Jiang, Q. High Catalytic Kinetic Performance of Amorphous CoPt NPs Induced on CeOx for H_2 Generation from Hydrous Hydrazine. *Int. J. Hydrogen Energy* **2014**, *39*, 3755−3761.

DOI: 10.1021/am5068436
ACS Appl. Mater. Interfaces 2015, 7, 1031−1034